The Formation of Stratlingite in Calcium Aluminate Containing Castable Systems

T. Shinmei, M. Ohkawa, A. Borovsky, M. Iiyama, Chr. Parr

The hydration mechanism of low cement castables has been long investigated but only a limited number of studies focused on specific hydrates are available. This paper will investigate a formation of stratlingite (C_2ASH_8), which is believed to prevent a conversion of metastable hydrates to the stable C_3AH_6 in high alumina cement-silica fume systems. The stratlingite formation at 21 °C and 35 °C was confirmed by XRD. Its early formation at higher curing temperature is accelerated by the addition of sodium tripolyphosphate as evidenced by XRD.

1 Introduction

A bonding matrix of low-cement castables (LCC) typically consists of high alumina cement (HAC) and silica fume (SF) [1–3]. Hardened LCC contain a range of calcium aluminate hydrates including CAH_{10}, C_2AH_8, C_4AH_{13}, C_4AcH_{11}, C_3AH_6, and C_2ASH_8 (stratlingite) [4–6]. C_2ASH_8 (stratlingite) is known as a hydrate stable over a long period of time [7–8]. The study aims to obtain a better understanding of the internal structure of the cement paste, its development over time and composition and the formation of stratlingite in simplified LCC systems.

The use of a siliceous material in combination with a sodium salt in CAC was recently reported to be more effective than the siliceous material alone in promoting formation of stratlingite [9] instead of hydrogarnet (C_3AH_6) [5, 7, 9, 10]. Siliceous materials, including natural zeolites, fly ash, slag and silica fume (SF) were effective in inhibiting the hydrogarnet formation and preventing strength reduction of CAC products when added in combination with a sodium salt. In particular, silica fume has been reported to favour the formation of stratlingite (C_2ASH_8) [11]. Silica fume reacts to form silicates in a high pH environment. This reaction is accelerated in the presence of an increased amount of alkali ions acting as a catalyst activating silica fume surfaces. Silicate anions then react with hydrated calcium aluminates to produce stratlingite [5].

Although the chemical analyses of stratlingites in castables had been reported by many researchers, the reported chemical data of stratlingite show a composition of non-uniformity [12–14]. This study investigates the formation and alteration of stratlingite in cement paste samples with or without defloccurant at two different curing temperatures, 21 °C and 35 °C. The nature, sequence, composition and microstructure of hydrated phases present in cement pastes consisting of CAC and SF with and without deflocculant were analyzed using X-ray diffraction (XRD), scanning electron microscopy (SEM) and electron probe microanalyzer (EPMA). Evolution of the cement paste hydration and a cause of changes in the hydrates in sealed glass bottles were determined by field emission scanning electron microscopy (FE-SEM) and energy dispersing X-ray analysis (EDX). Since stratlingite formation also occurs in LCC after a long curing time, and is considered to inhibit a hydrogarnet formation, it is also the aim of the present work to shed more light on the mechanism of LCC hardening [15].

Tab. 1 Chemical composition of CAC and silica fume [mass %]

	L.o.I.	SiO_2	Al_2O_3	Fe_2O_3	TiO_2	CaO	MgO	Na_2O	K_2O	C
CAC	0,14	0,21	69,49	0,17	0,02	29,79	0,27	0,21		
SF	0,50	98,4	0,20	0,01		0,20	0,10	0,15	0,20	0,50

2 Experimental

Materials used in this study included Secar 71, a 70 % alumina cement (CAC), produced by *Kerneos;* commercially available silica fume (SF) Elkem 971-U produced by *Elkem Materials;* and reagent grade sodium tripolyphosphate (TPP). Chemical composition of raw materials as provided by the

Toshio Shinmei, Makio Ohkawa
Department of Earth and Planetary Systems Science, Faculty of Science, Hiroshima University
Hiroshima 739-8526
Japan

Adriana Borovsky
Kerneos do Brasil
24722-030 Sao Gonçalo
Rio de Janeiro
Brazil

Makoto Iiyama
Kerneos Japan
Tokyo 103-0007
Japan

Chris Parr
Kerneos France
92521 Neuilly sur Seine Cedex
France

Corresponding author: *Chris Parr*
E-mail: chris.parr@kerneos.com

Keywords: calcium aluminate cement, stratlingite, deflocculant, silica fume, sodium tripolyphosphate, hydrates, EPMA, SEM

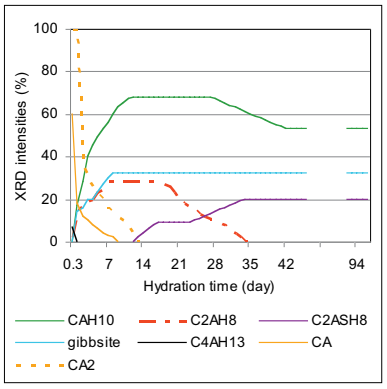

Fig. 1 XRD results of sample hft-21

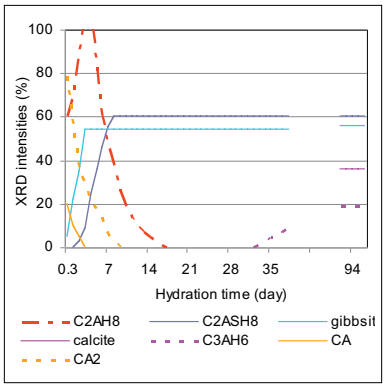

Fig. 2 XRD results of sample hft-35

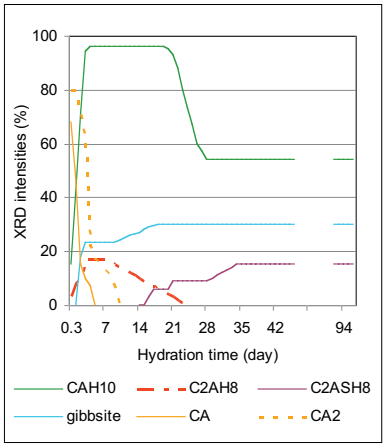

Fig. 3 XRD results of the sample hf-21

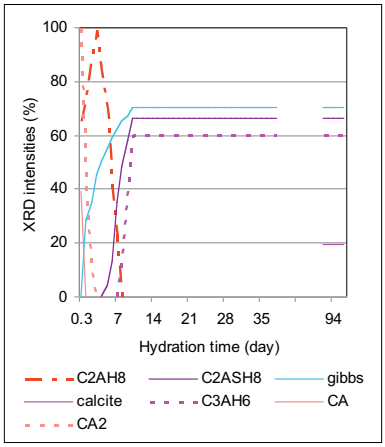

Fig. 4 XRD results of the sample hf-35

manufacturers is presented in Tab. 1. The main mineralogical phases of CAC are CA ($CaO \cdot Al_2O_3$) and CA_2 ($CaO \cdot 2Al_2O_3$) as evident from X-ray diffraction analysis in which the cardinal constituent is corundum (Al_2O_3). Silica fume has an average particle size less than 1 µm.

Cement paste samples with 60 mass-% of CAC and 40 mass-% of SF were prepared by mixing the required amounts of solids and deionized water at a water/solid ratio of 0,864 for 3 min 0,41 mass-% of TPP was dissolved in a required amounts of water in advance, and then the water was mixed into the solid sample. The freshly mixed cement paste was placed into small glass bottles (ϕ 20 × h 40 mm), and then sealed with a plastic lid, These bottle samples were divided into two groups; one group was placed in a 21 ± 2 °C water-bath while the other in a thermostatic oven at the temperature of 35 ± 1 °C.

After 2 days of curing, each bottle sample was split into several fragments of about 0,5–1,5 cm^3. These fragments were then reinserted into a new glass bottle with a water-soaked cotton ball placed inside and sealed with a plastic lid, In this way the atmosphere above the paste was approximately saturated with water vapour, and the heat of reaction was quickly conducted away from the sample. The repackaged samples were cured for a predetermined period of time under the same conditions as before, i.e. at 21 ± 2 °C or at 35 ± 1 °C. Subsequently, a designated quantity was cut daily from the surface of a sample stored in a bottle, washed in acetone to stop the hydration [6] and air-dried before being analyzed.

In this paper, the prepared cement paste samples were labeled hf and hft (h for high alumina cement = CAC, f for SF and t for TPP), numbers 21 and 35 are a reference of the curing temperature.

2.1 XRD (X-ray Diffraction) analyses

RIGAKU MultiFlex X-ray diffractometer was used, Copper Kα radiation with λ = 0,15418 nm at 40 kV and 40 mA was employed. The fragment samples (the total amount of 0,300 g) were taken with a spatula from the bottles, and then the samples were ground to a fine powder (<63 µm) in acetone. A special reagent grade of corundum (Al_2O_3) was used as the reference material for intensity and d-spacing, 10 mass-% of the reagent was mixed into the powdered sample, X-ray analyses were done at the predetermined periods as follows: 8 h later, every day in the first week, weekly during the following six weeks, and 94 days later.

2.2 EPMA (Electron Probe Microanalysis) analyses

Samples of about 5–8 mm in size, hydration of which was stopped by acetone, were prepared after 27 days and embedded in a resin, then polished half way through to expose a cross-section of the material. In order to prevent further hydration a liquid lubricant DP-Lubricant Blue *(Struers Corp)* was used, EPMA was carried out for analyses of the following 9 components: SiO_2, CaO, Fe_2O_3, Al_2O_3, P_2O_5, Na_2O, K_2O, MgO, and TiO_2, using a JEOL JXA-8200 EPMA with an accelerating voltage of 15 kV, a beam current of 5 nA, and a spot size of 3 µm. Back-scattered electron (BSE) imaging was also conducted. Note that the measurement was performed 9 days after the acetone treatment.

2.3 SEM (Scanning Electron Microscopy) analyses

The polished samples used for the EPMA measurement were trimmed to 9 mm × 5 mm fractions for FE-SEM *(Hitachi S-5200)* analyses. Chemical analyses were carried out by the EDX (EDAX Genesis XM2) X-ray analyzer. The measurement was performed 114 days after the acetone treatment,

3 Results and discussion

3.1 XRD analyses

Samples cured at 21 °C with TPP (hft) and without TPP (hf) were left to harden for about 8 h while those samples at 35 °C for about 6 h before they were analyzed.

(1) CAH_{10}

CAH_{10} hydrate was detected only in the samples cured at 21 °C as shown in Figs. 1 and 3, In the samples cured at 35 °C this hydrate was converted as evidenced from Fig. 2 and 4, CAH_{10} has been detected along with C_2AH_8 in hf-21 without TPP since the beginning of curing (Fig. 3) but in the samples

with TPP, both hydrates crystallized only after 1 day (Fig. 1). From curves depicted in Fig. 1 and 3 it is evident that there is an increase in the CAH_{10} peak intensity over time in the samples without TPP until an abrupt drop is observed, followed by a plateau. Samples with TPP give more gradual curves, the XRD intensity in the figures was a quotient value of the higher peak of the component for that of the reference material (corundum).

(2) C_2AH_8

The C_2AH_8 hydrate has crystallized in large quantities in the samples cured at 35 °C with or without TPP since the beginning of curing (Fig. 2 and 4). Other trend was observed in the samples cured at 21 °C (Fig. 1 and 3)., In general, in samples with TPP the C_2AH_8 peak lasts longer and is also slightly stronger but as one observes, especially at higher curing temperature, the peak disappears more quickly. The descending curve of C_2AH_8 is crossing an ascending curve of stratlingite as formation of stratlingite is preceded by the formation of meta-stable C_2AH_8 [13].

(3) C_4AH_{13}

C_4AH_{13} hydrate was detected for a short period of time in hft-21, and then completely disappeared after 1 day. Although C_4AH_{13} is described as a transient hydrate for C_4ACH_{11} and C_3AH_6 hydrates [11], such end products were not detected in this study.

(4) C_2ASH_8

As evident from Fig. 1–4, stratlingite crystallized precociously in the samples cured at higher temperature and with TPP. TPP is available because its sodium ions have a significant influence on stratlingite formation [10]. Mineralogical phases CA and CA_2 (Fig. 1–4) disappeared more rapidly at higher curing temperature while their dissolution is slightly delayed at lower curing temperature. This delay in dissolution of CAC, through addition of TPP, seemed to slightly speed up the stratlingite formation.

(5) $Al(OH)_3$

Gibbsite [$Al(OH)_3$] was detected in hft-35 already after 6 h, At 35 °C its peak intensity increases rapidly before a plateau is reached.

(6) C_3AH_6

C_3AH_6did not crystallize in samples cured at 21 °C. In hf-35 without TPP C_3AH_6 was detected after 9 days. In hft-35 with addition of TPP its crystallization was delayed and occurred only after 5 weeks.

Tab. 2 Results of EPMA analyses

	Molar Ratio				
	CaO	Al_2O_3	SiO_2	H_2O	Phase
P1	0,98	1,00	0,05	7,32	CAH_{10}
P2	0,99	1,00	0,00	0,18	_ _ _ _
P3	1,81	1,00	1,17	7,51	C_2ASH_8
P4	1,70	1,00	2,74	6,81	_ _ _ _ _
P5	1,80	1,00	3,93	7,60	_ _ _ _ _
P6	2,18	1,00	0,10	6,32	C_2AH_8
P7	2,02	1,00	0,35	6,05	C_2AH_8
P8	1,96	1,00	0,38	6,01	C_2AH_8
P9	1,29	1,00	0,13	4,15	CAH_
P10	1,89	1,00	4,48	7,18	_ _ _ _ _
P11	1,83	1,00	2,82	5,95	_ _ _ _ _ 8
P12	1,88	1,00	3,46	6,16	_ _ _ _ _ 8
P13	1,82	1,00	3,71	7,19	_ _ _ _ _
P14	1,86	1,00	3,97	7,32	_ _ _ _ _
P15	1,84	1,00	4,16	7,68	_ _ _ _ _
P16	1,74	1,00	3,99	7,68	_ _ _ _ _
P17	1,76	1,00	3,34	7,07	C _ A S _ H
P18	1,70	1,00	3,03	7,46	_ _ _ _ _
P19	0,76	1,00	42,30	112,97	SF
P20	0,16	1,00	3,07	1,69	SF + A1
P21	1,37	1,00	2,94	5,71	CAS_H
P22	1,32	1,00	2,66	5,53	CAS_H
P23	1,18	1,00	2,67	5,18	CAS_H
P24	1,64	1,00	3,23	7,48	_ _ _ _ _
P25	1,92	1,00	3,02	5,78	C_AS_H
P26	1,83	1,00	3,81	5,80	C_AS_H
P27	0,40	1,00	36,60	36,27	SF
P28	1,74	1,00	3,18	6,24	C_AS_H
P29	1,79	1,00	2,10	6,78	C_AS_H
P30	1,52	1,00	3,08	6,96	C_AS_H
P31	1,84	1,00	1,12	6,89	C_2ASH_8
P32	0,51	1,00	35,34	77,88	SF
P33	1,98	1,00	0,91	7,33	C_2ASH_8
P34	1,90	1,00	3,35	7,15	C_AS_H
P35	2,79	1,00	1,57	5,65	C_ASH

(7) $CaCO_3$

Regardless of the TPP presence, calcite ($CaCO_3$) was identified only in the samples cured at 35 °C after 3 months. This is a consequence of atmospheric CO_2 inside a glass bottle and its reaction with stratlingite and C_3AH_6 leading to their carbonation.

3.2 EPMA analyses

The EPMA analyses are shown in Tab. 2. The water content was calculated assuming that all the residues were water molecules, BSE images reveal large masses of SF of about 100~200 µm in diameter on a rough surface of bottle samples.

Hft-21 represented by sample P1–P12 in Tab. 2

A number of features can be identified from the BSE images (not shown). The space between the masses is filled with plate crystals and an amorphous material. Furthermore, big crystals of different hydrates are often surrounded by SF masses. The samples appear to have heterogeneous texture. Analyses of the grey part (P1) reveals that it is CAH_{10} and an irregularly shaped white area (P2) is an unhydrated CAC. EPMA analyses of a smooth part (P3) of bulky white-gray crystals show that its composition is close to the stratlingite composition

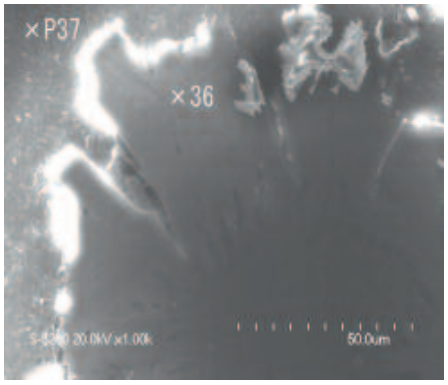

Fig. 5a

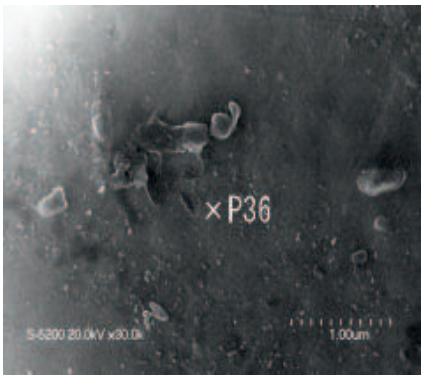

Fig. 5b

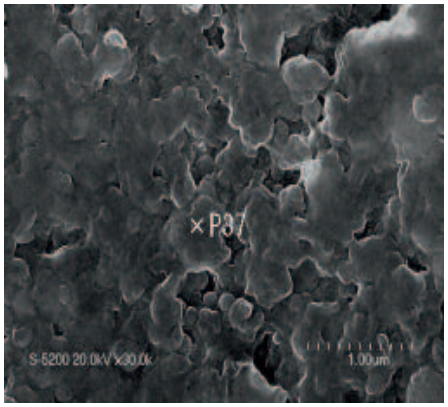

Fig. 5c

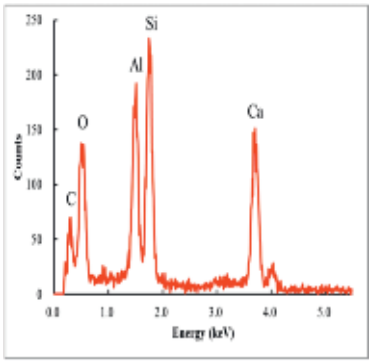

Fig. 5d

Fig. 5 SEM image of the sample hf-35: (a) a radiated massive crystal, (b) a crystal surface around P36, (c) irregularly shaped grains of the SF hydrate, and (d) EDX analyses in P36

($CaO:Al_2O_3:SiO_2:H_2O = 2:1:1:8$) while in a rough part (P4) a slightly lower molar ratio of CaO and a higher molar ratio of SiO_2 were calculated (Tab. 2). The analyses of P5 also confirm a slightly lower molar ratio of CaO and higher SiO_2. The analyses of P6 where well-developed plate-like crystals are visible indicates C_2AH_8 while analyses of P7 and P8 suggest that some SiO_2 adhered to the C_2AH_8 crystals. Based on the area calculations, the gray-white area (P9) in the corresponds to CAH_{10}. However, XRD did not detect any CAH_{10} possibly because these crystals disappear by converting to the fine C_2AH_8 crystals. P10–12 were taken from the edge of a large mass of SF of about 100 µm in diameter of round-shaped crystals. Analyses of these crystals in P10, P11 and P12 indicate stratlingite with a slightly lower molar ratio of CaO, and higher molar ratio of SiO_2.

Hf-21 represented by samples P13–P24 in Tab. 2

P13–18, P24 represent bulky hydrates of 50 µm in diameter or more around large chunks of SF. Analyses of these crystals indicate stratlingite with a slightly lower molar ratio of CaO and much higher of SiO_2. In P21–23 the CAH_{10} hydrate seems to be infiltrated with SiO_2 as suggested from its higher molar ratio. It was found that the SF mass is contaminated with a dense substance composed of SiO_2 (P19) and fine grains of alumina (P20).

Hf-35 represented by samples P25–P35 in Tab. 2

These samples reveal quite big crystals inside and at the edge of SF masses. Composition of these crystals in P25, P26, P28, P29 indicates that they are stratlingite with a low molar ratio of CaO and high SiO_2, P31 and P33 of the large crystals exhibit the composition which is close to stratlingite while P30 and P34 have a lower molar ratio of CaO and a higher molar ratio of SiO_2. Big chunks were confirmed to be composed of SF in P27 and in P32, P35 represents small white-grey grains in the matrix, analyses of which correspond to C_3AH_6 incorporating some SiO_2. However, XRD did not confirm the presence of hydrogarnet (C_3AH_6).

3.3 SEM

The composition of crystalline hydrate indicates C_2ASH_8 with a high SiO_2 molar ratio mainly probably because (1) fine crystals of C_2ASH_8 are surrounded by unreacted SF [11], or (2) C_2ASH_8 crystals are contaminated with silicates[11], or (3) amorphous silica is attached to the surface of C_2ASH_8 crystals. A previous study [14], does not provide an evidence for statements (1) and (2).

In this study the surface of C_2ASH_8 crystals with a high SiO_2 molar ratio was observed by FE-SEM and is shown in Fig. 5a–c. The SEM image of the area near P36 shows (Fig. 5b) irregularly shaped grains of about 0,5 µm clearly attached to the surface. They were found to be composed of SF. These grains of SF can increase the SiO_2 molar ratio of surface (Fig. 5d), and as such a possibility of these structures cannot be denied. Outside of the crystals there is a chunk of SF. SEM image (Fig. 5c) shows irregularly shaped particles of less than 0,5 µm covered in a gelatinous substance. EDX elemental analyses of P37 detected mostly Si and some Al with some residual quantity of Ca. In the center of well-developed plate-like crystals, a smooth matrix is visible (Fig. 6a). Its surface was magnified up to 300 000 but any adhesion/attachment of SF particles was not recognized (Fig. 6b). The EDX elemental analyses of P38 (Fig. 6c) indicate molar ratios of main components are close to C_2ASH_8. However, a flat side of the polished surface is very small for any detailed observation.

4 Conclusions

CAC pastes with SF some containing TPP were mixed. The paste was then cast into a bottle and cured at 21 °C and 35 °C. Development of different hydrates over time was analyzed by XRD and during the final stages, by EPMA, some selected samples were observed by EPMA and FE-SEM.

10TH INDIA INTERNATIONAL REFRACTORIES CONGRESS

IREFCON14

JANUARY 15-18, 2014
HOTEL TAJ BENGAL
KOLKATA, INDIA

Congress Theme: Refractories Solutions Through Innovations

Keynote Address: Prof. C.G. Aneziris,
Technical Univ. of Freiberg, Germany

Block Your Dates Today!!

Contact:
Email: irmaindia@hotmail.com
indrefractory@yahoo.co.in
Web: http://www.irmaindia.org/irefcon/

IRMA

ATTENDED BY MORE THAN 500 DELEGATES WORLDWIDE

Fig. 6a

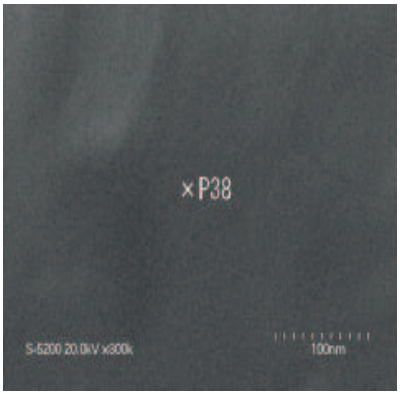

Fig. 6b

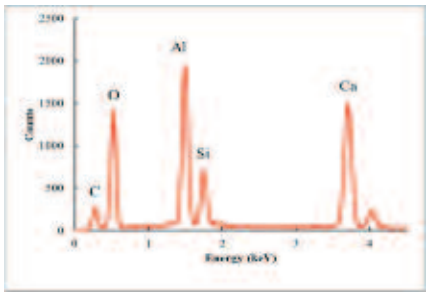

Fig. 6c

Fig. 6 SEM image of the sample hf-35: (a) the platy crystal with a smooth surface, (b) the zoomed image of a surface around P38, and (c) EDX analyses in P38

- The hardening of samples with TPP, regardless on the curing temperature, was delayed but the early crystallization of stratlingite was observed because of the presence of sodium ions. The stratlingite formation was further accelerated at higher curing temperature.
- C_2AH_8 has crystallized in all samples since the beginning of hydration. The higher the curing temperature, the higher is its X-ray peak intensity. It soon started to disappear and crystallization of stratlingite was observed as the C_2AH_8 hydrate was found to convert to stratlingite.
- After three months of curing at 21 °C, regardless of the TPP presence, in addition to CAH_{10}, gibbsite and stratlingite were detected, C_3AH_6 and calcite were not detected. In samples without TPP cured at 35 °C, C_3AH_6 crystallized along with gibbsite and stratlingite, calcite was also de-

tected. When TPP was added, in addition to stratlingite and gibbsite. C_3AH_6 and calcite were detected at later stages.

- EPMA analyses showed that SF developed in and around large plate-like crystals with a smooth surface that match with the composition of stratlingite. The analyses of what appears to be a rough surface show variations in a molar ratio of SiO_2, mainly higher molar ratio.
- FE-SEM images show that a rough surface of big plate-like crystals is covered with small grains of SF. These plate crystals were indentified by EDX analyses as stratlingite containing a higher SiO_2 molar ratio. This higher molar ratio of SiO_2 can be explained by the presence of these SF grains.

This study aimed to gain a better understanding of the internal structure of the cement paste, its development over time and composition. However, the surface area of cement paste is subjected to different chemical alterations than its interior. Generally, efflorescence occurs on a surface of the cement paste. Further studies will aim at investigating the effect of atmosphere and CO_2 on stratlingite.

Acknowlegements

The authors thank *Prof. H. Hidaka* of the Hiroshima University for his advice and guidance. Thanks also to *Prof. K. Terada* and *Dr. J. Ando* of the same university for their valuable comments, and to *Y. Shibata* of the same university for his help with the *EPMA* analysis. This study was supported by research grants from Kerneos.

References

[1] Lee, W.E.; Moore, R.E.: The evaluation of in situ refractories in the 20th century. J. Amer. Ceram. Soc. **81** (1998) [6] 1385–1410

[2] Daspoddar, D.; Das, S.K.; Daspoddar, P.K.: Effect of silica sol of different routes on the properties of low cement castables. Bull. Mater. Sci. **26** (2003) [2] 227–231.

[3] Antonovic, V.; et al.: A review of the possible applications of nanotechnology in refractory concrete. J. Civil Engin. and Management **16** (2010) [4] 594–602

[4] Cong X.; Kirkpatrick R. J.: Hydration of calcium aluminate cements: A solid-state 27Al NMR study. J. Amer. Ceram. Soc. **76** (1993) [2] 409–416

[5] Ding, J.; Fu, Y.; Beaudoin, J.J.: Stratlingite formation in high alumina cement – silica fume systems: Significance of sodium ions. Cem. Concr. Res. **25** (1995) [6] 1311–1319

[6] Ding, J.; Fu, Y.; Beaudoin, J.J.: Study of hydration mechanisms in the high alumina cement – sodium silicate system. Cem. Concr. Res. **26** (1996) [5] 799–804

[7] Fu, Y.; Ding, J.; Beaudoin, J.J.: Conversion-preventing additive for high alumina cement products. US Patent 5624489 (1997)

[8] Rayment, D.L.; Majumdar, A.J.: Microanalysis of high-alumina cement clinker and hydrated HAC/slag mixtures. Cem. Concr. Res. **24** (1994) [2] 335–342

[9] Majumdar, A.J.; Singh, B.: Properties of some blended high-alumina cements. Cem. Concr. Res. **22** (1992) [6] 1101–1114

[10] Edmonds, R.N.; Majundar, A.J.: The hydration of mixtures of monocalcium aluminate and blastfurnace slag. Cem. Concr. Res. **19** (1989) [5] 779–782

[11] Bentsen, S.; Seltveit, A.; Sandberg, B.: Calcium Aluminate Cements, E.&F.N. SPON (1990) 294–319

[12] Kumar, S.; Das, S.K.; Daspoddar, P.K.: Thermo mechanical behaviour of low cement castable derived from mullite aggregates synthesized from beach sand sillimanite. Ceram. Int. **29** (2003) 671–677.

[13] Sarpoolaky, H.; Ahari, K.G.; Lee, W.E.: Influence of in situ phase formation on microstructural evolution and properties of castable refractories. Ceram. Int. **28** (2002) [5] 487–493

[14] Shinmei, T.; et al.: Stratlingite in hydrate of high alumina cement with silica fume. Taikabutsu **62** (2010) [2] 75–80

[15] Maeda, E.: Analysis of setting mechanism of low-cement castables (III): The acceleration of the setting by addition of Ca^{2+} ions. Taikabutsu **62** (2010) [6] 280–290

Developing the Powder Metallurgy Future

european powder
metallurgy association

EPMA
european powder metallurgy association

ADVANCED REGISTRATION DEADLINE - 31 JULY

LIMITED EXHIBITION SPACE AVAILABLE

EURO PM2013 CONGRESS & EXHIBITION

15 - 18 September 2013

Svenska Mässan, The Swedish Exhibition and Congress Centre, Gothenburg, Sweden

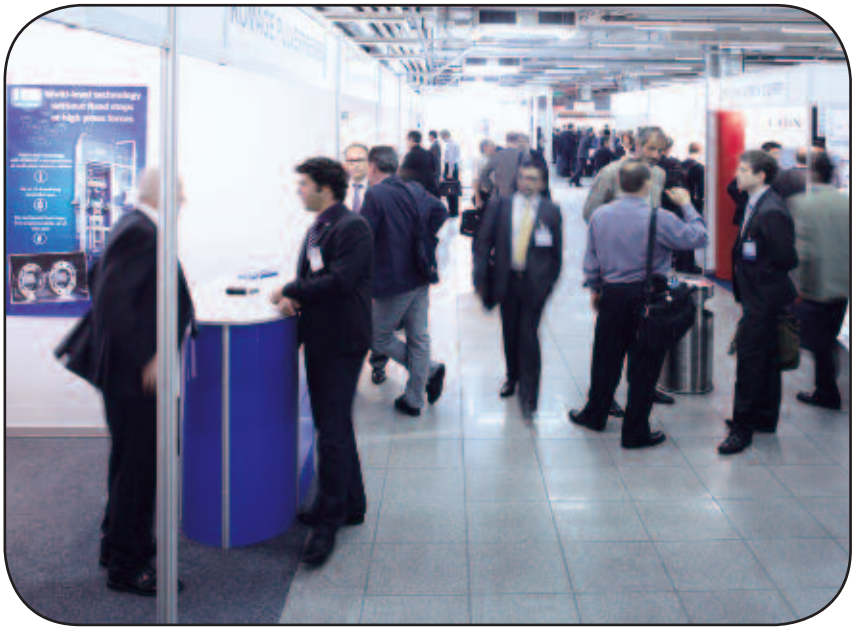

An all topic powder metallurgy event focusing on:

- Structural Parts PM
- Hard Materials and Diamond Tools
- Hot Isostatic Pressing
- New Materials and Applications
- Powder Injection Moulding
- **NEW for 2013** Additive Manufacturing

Including New Keynote Papers Awards

www.epma.com/pm2013

EURO PM2013 congress & exhibition